Earth Syst. Dynam. Discuss., https://doi.org/10.5194/esd-2017-107
Manuscript under review for journal Earth Syst. Dynam.
Discussion started: 27 November 2017

Earth System Dynamics
Discussions
Open Access
EGU

Midlatitude atmospheric circulation responses under 1.5 °C and 2.0 °C warming and implications for regional impacts

Camille Li[1,2], Clio Michel[1,2], Lise Seland Graff[3], Ingo Bethke[4,2], Giuseppe Zappa[5], Thomas J. Bracegirdle[6], Erich Fischer[7], Ben Harvey[5], Trond Iversen[3], Martin P. King[4,2], Harinarayan Krishnan[8], Ludwig Lierhammer[9], Daniel Mitchell[10], John Scinocca[11], Hideo Shiogama[12], Dáithí A. Stone[8,13], and Justin J. Wettstein[14,1,2]

[1]Geophysical Institute, University of Bergen, Bergen, Norway
[2]Bjerknes Centre for Climate Research, Bergen, Norway
[3]Norwegian Meteorological Institute, Oslo, Norway
[4]Uni Climate, Uni Research, Bergen, Norway
[5]Department of Meteorology, University of Reading, Reading, UK
[6]British Antarctic Survey, Cambridge, UK
[7]Institute for Atmospheric and Climate Science, ETH Zürich, Zürich, Switzerland
[8]Lawrence Berkeley National Laboratory, Berkeley, CA, USA
[9]German Climate Computing Center (DKRZ), Hamburg, Germany
[10]School of Geographical Sciences, University of Bristol, Bristol, UK
[11]Canadian Centre for Climate Modelling and Analysis, Environment and Climate Change Canada, Victoria, Canada
[12]National Institute for Environmental Studies, Tsukuba, Japan
[13]Global Climate Adaptation Partnership, Oxford, UK
[14]College of Earth, Ocean, and Atmospheric Sciences, Oregon State University, Corvallis, USA

Correspondence to: Camille Li (camille@uib.no)

Abstract.

This study investigates the global response of the midlatitude atmospheric circulation to 1.5°C and 2.0°C of warming using the HAPPI "Half a degree Additional warming, Projections, Prognosis and Impacts" ensemble, with a focus on the winter season. Characterizing and understanding this response is critical for accurately assessing the near-term regional impacts of climate change and the benefits of limiting warming to the 1.5°C above pre-industrial levels, as advocated by the Paris Agreement of the United Nations Framework Convention on Climate Change (UNFCCC). The HAPPI experimental design allows an assessment of uncertainty in the circulation response due to model dependence and internal variability. Internal variability is found to dominate the multi-model mean response of the jet streams, storm tracks and stationary waves across most of the midlatitudes; larger signals in these features are mostly consistent with those seen in more strongly forced warming scenarios. Signals that emerge in the 1.5°C experiment are a weakening of storm activity over North America, an inland shift of the North American stationary ridge, an equatorward shift of the North Pacific jet exit, and an equatorward intensification of the South Pacific jet. Signals that emerge under an additional 0.5°C of warming include a poleward shift of the North Atlantic jet exit, an eastward extension of the North Atlantic storm track, and an intensification on the flanks of the Southern

Earth Syst. Dynam. Discuss., https://doi.org/10.5194/esd-2017-107
Manuscript under review for journal Earth Syst. Dynam.
Discussion started: 27 November 2017

Earth System Dynamics
Discussions
Open Access
EGU

Hemisphere storm track. Case studies explore the implications of these circulation responses for precipitation impacts in the Mediterranean, western Europe and the North American west coast, paying particular attention to possible outcomes at the tails of the response distributions. For example, the projected weakening of the Mediterranean storm track emerges in the 2° world, though the ensemble spread still allows for both wetting and drying responses.

1 Introduction

There is growing urgency to understand the near-term impacts of climate change for low-end warming targets. This need arises from the Paris Agreement's aim to "strengthen the global response to the threat of climate change by keeping a global temperature rise this century well below 2 degrees Celsius above pre-industrial levels and to pursue efforts to limit the temperature increase even further to 1.5 degrees Celsius" (UNFCCC, 2015). In order to better assess the associated impacts, the scientific community devised the "Half a degree Additional warming, Projections, Prognosis and Impacts" (HAPPI) initiative (Mitchell et al. (2017); `http://www.happimip.org/`).

The purpose of this study is to examine the midlatitude atmospheric circulation response in the HAPPI experiments, which represent worlds that are 1.5°C and 2.0°C warmer than pre-industrial conditions (or 0.7°C and 1.2°C warmer than present conditions; see section 2). The HAPPI experiments were designed to quantify the potential benefits of a mitigation effort to reduce warming by an extra half a degree, i.e., the climate impacts avoided by limiting warming to 1.5°C compared to 2.0°C (Mitchell et al., 2017). They are inspired by experiments in existing and planned international initiatives (e.g., International CLIVAR Climate of the 20th Century Plus Detection and Attribution, C20C+ D&A) focused on extreme weather events (Folland et al., 2014; Stone et al., in prep 2017). For the purposes of this study, two aspects of the HAPPI experiments bear mention. First, the use of large ensembles allows an investigation of the spread in the responses, in particular, changes in the tails and shapes of their distributions. This is especially important when the responses of interest are related to the midlatitude atmospheric circulation, which features large internal variability (Deser et al., 2012; Shepherd, 2014). Second, the use of common sea surface temperature and sea ice conditions allows us to isolate the consensus atmospheric response across models.

Despite the expectation that the mean response of the midlatitude atmospheric circulation will be weak in these experiments, the present study nevertheless furnishes critical baseline knowledge for the HAPPI project. Specifically, it documents the large-scale background climate changes being used to compute indices for extreme events and as input for impact models (e.g., Baker, in review 2017; Jacob et al., submitted 2017; Mitchell, in review 2017; Shiogama, submitted 2017; Wehner et al., in review 2017). In this way, it provides information that can help inform, interpret and corroborate results of other, more impacts-focused, HAPPI studies.

Earth Syst. Dynam. Discuss., https://doi.org/10.5194/esd-2017-107
Manuscript under review for journal Earth Syst. Dynam.
Discussion started: 27 November 2017

Section 2 briefly describes the philosophy of the HAPPI experiments, the experimental setup, and model output, as well as the statistical framework used to analyze the HAPPI ensemble. Section 3 presents the multi-model mean circulation responses under 1.5°C of warming and the additional 0.5°C of warming, with a focus on the wintertime, the season during which midlatitude dynamics – and the associated poleward energy transport – are most vigorous. Section 4 presents case studies to illustrate possible implications of the model results for regional climate change by looking beyond the multi-model mean responses to the spread in the responses (in essence, by exploring precipitation changes associated with outcomes at the tails of the response distributions). Finally, section 5 raises some discussion points and concluding remarks. In addition, a supplement contains figures showing the model biases compared to ERA-Interim reanalysis data (Dee et al. (2011); S1), the multi-model mean responses for the summer season (S2), and the 2.0°C response relative to present climate (S3).

2 Methods and data

2.1 Experimental setup

The HAPPI modelling experiments allow the investigation of atmospheric responses under weak warming scenarios, their associated uncertainties, and the resulting impacts. The experiments follow a protocol similar to current (and proposed) climate experiments, particularly those within the International CLIVAR Climate of the 20th Century Plus Detection and Attribution (C20C+ D&A) project (Folland et al., 2014; Stone et al., in prep 2017), to best exploit synergies. In contrast to scenarios based on emissions or greenhouse gas concentration trajectories used by the Coupled Model Intercomparison Project (CMIP), the HAPPI approach is based on a global temperature constraint, and uses large ensembles to allow for comparison of extremes and to feed into impact models (see Fig. 1 in Mitchell et al., 2017).

Mitchell et al. (2017) document the setup of the Tier 1 HAPPI experiments, performed using the atmosphere-only models listed in Table 1. The three Tier 1 experiments simulate a present decade (PD, 2006–2015), a decade that is 1.5°C warmer than pre-industrial conditions (approximately 0.7°C warmer than PD), and a decade that is 2.0°C warmer than pre-industrial conditions (approximately 1.2°C warmer than PD).

Ensemble members within each experiment are 10-year long simulations differing only in their initial conditions. They are forced with time-varying sea surface temperature (SST), sea ice and anthropogenic radiative forcings (due to greenhouse gases, aerosols, land use, land cover) estimated for the period of interest (PD, 1.5°C or 2.0°C). Natural radiative forcings are prescribed according to observed PD values in all three experiments. The future experiment forcings are calculated using output from the lower end RCP2.6 and RCP4.5 scenarios, which produce a global mean temperature response at the end of the century (2091–2100) of approximately 1.5°C and 2.5 °C, respectively,

Earth Syst. Dynam. Discuss., https://doi.org/10.5194/esd-2017-107
Manuscript under review for journal Earth Syst. Dynam.
Discussion started: 27 November 2017

above pre-industrial levels (Fig. 2 in Mitchell et al., 2017; Collins et al., 2013). All models include active land components such that surface temperature over land points is not fixed.

The main setup points for the three experiments are listed below; additional details on how the forcings were constructed can be found in Mitchell et al. (2017).

- Present decade (PD) experiment: Observed SST, sea ice, atmospheric greenhouse gas concentrations, aerosols, ozone, land use and land cover for present conditions (2006–2015) are used.

- 1.5°C experiment: SST changes, calculated as the difference between a 1.5°C world (RCP2.6 scenario over the period 2091–2100) and the present decade (RCP8.5 scenario over the period 2006–2015), are added to the PD SSTs. Sea ice concentrations are adjusted for consistency with the warmer SSTs. Atmospheric greenhouse gas concentrations, aerosols, ozone, land use and land cover are set to 2095 values from RCP2.6.

- 2.0°C experiment: SST and sea ice cover are calculated in a similar way to those for the 1.5°C experiment, except that changes are determined using a weighted sum of the RCP2.6 and RCP4.5 scenarios over the period 2091–2100 to correspond to a 2.0°C world. Atmospheric CO_2 concentrations are set to a weighted average of values from RCP2.6 and RCP4.5 in the 2.0°C experiment; other atmospheric greenhouse gases, aerosols, ozone, land use and land cover are set to 2095 values from RCP2.6.

Monthly variables used in the study are surface air temperature (K), precipitation (mm d^{-1}), zonal wind at 850 hPa ($u850$, m s^{-1}), zonal wind at 250 hPa ($u250$, m s^{-1}), meridional wind at 250 hPa ($v250$, m s^{-1}), geopotential height at 500 hPa ($Z500$, m) and temperature at 850 hPa and 200 hPa ($T850$ and $T200$, K). Stationary waves are calculated as departures from the zonal mean ($Z500*$, $v250*$). Daily variables are filtered with a 2–6 day bandpass filter to isolate synoptic-scale variability in mean sea level pressure (MSLP′, hPa), zonal wind at 250 hPa ($u250'$, m s^{-1}) and meridional wind at 250 hPa ($v250'$, m s^{-1}). These are used to calculate storm track metrics: the low-level storm tracks are defined as the standard deviation of MSLP′, and the upper level storm tracks are defined via eddy kinetic energy (EKE $= u250'^2 + v250'^2$, m^2 s^{-2}). Model biases of the PD experiment compared to ERA-Interim are shown in the supplement (S1).

The temperature responses are consistent with those from the RCP scenario simulations performed under CMIP5 (see Fig. 12.12 Collins et al., 2013). Maps of surface air temperature responses (Fig. 1 look reasonable relative to the RCP scenarios (Collins et al., 2013), featuring the expected amplification of warming over land and in the Arctic. Model consensus on the magnitude of the response improves over high latitude regions with the additional 0.5°C of warming, indicated by the reduction in dots in 2.0°C−PD (Fig. S3.1a) and even 2.0°C−1.5°C (Fig. 1b) compared to 1.5°C−PD (Fig. 1a). The troposphere generally warms due to increased greenhouse gas concentrations, with

Earth Syst. Dynam. Discuss., https://doi.org/10.5194/esd-2017-107
Manuscript under review for journal Earth Syst. Dynam.
Discussion started: 27 November 2017

Earth System Dynamics
Discussions
Open Access
EGU

Table 1. Models used in study, including the number of ensemble members run for each of the PD, 1.5°C and 2.0°C experiments.

Model	Horizontal resolution	Vertical levels	Members / experiment	References
CAM4	1.9° × 2.5°	26	501	Neale et al. (2013)
CanAM4	T63 (96 × 192)	35	100	von Salzen et al. (2013)
MIROC5	T85 (128 × 256)	40	100	Shiogama et al. (2013)
ECHAM6.3-LR	T63 (96 × 192)	47	100	Lierhammer et al. (2017)
NorESM1-Happi	0.94° × 1.25°	26	125	Bentsen et al. (2013)
				Iversen et al. (2013)
				Kirkevåg et al. (2013)

stronger near-surface warming in the Arctic and stronger upper tropospheric warming in the tropics, and the stratosphere cools (not shown).

2.2 ANOVA framework

The HAPPI multi-model ensemble is analaysed and interpreted using the two-way analysis of variance ANOVA framework introduced in Sansom et al. (2013). Each model's climate change response is computed as the difference between the future (1.5°C or 2.0°C) and present (PD) mean climate, which is estimated by averaging across all the available ensemble members for each model (see Table 1). The multi-model mean response (β) is then obtained as the average of the individual models' future responses.

The signal-to-noise ratio in the climate change response (β/σ) is evaluated relative to the noise due to internal decadal climate variability (σ; decadal because each ensemble member is a 10-year simulation). Following Sansom et al. (2013), one value of σ is obtained for the whole multi-model ensemble by pooling together variations in decadal mean climate across all the ensemble members. A signal-to-noise ratio β/σ greater than 1 implies that the amplitude of the climate change response is larger than decadal climate variability, suggesting a substantial climatological impact in the region. A β/σ less than 1 implies that internal variability dominates, but there could still be a non-negligible impact depending on the region.

Finally, a measure of consensus on the magnitude of the climate change response is estimated via the metric f^2. This represents the ratio of the uncertainty in the future response due to the model dependence (differences in response from model to model) compared to the uncertainty due to internal (decadal) climate variability (see Sansom et al., 2013, for details). We interpret $f^2 < 1$ as evidence of consensus on the magnitude of the climate change response, as this implies that internal climate variability is the dominant source of uncertainty in the multi-model projections.

Earth Syst. Dynam. Discuss., https://doi.org/10.5194/esd-2017-107
Manuscript under review for journal Earth Syst. Dynam.
Discussion started: 27 November 2017

The multi-model mean precipitation results for 1.5°C of warming (1.5°C−PD) and an additional 0.5°C of warming (2.0°C−1.5°C) are shown in Figure 2 for winter, and in Figure 3 for summer. The top panels show multi-model mean response β. In shading in the bottom panels is the signal-to-noise ratio β/σ, where the sign corresponds to the sign of the response. The patterns of β/σ and β are similar, but relative magnitudes between locations can differ if the spread associated with decadal variability is very different. Model consensus on the magnitude of the response is generally good, even where the response β is weak, with only a few locations showing poor consensus (e.g., black dots in the Canadian Archipelago, Kara Sea, Caspian Sea). Note that a location with high signal-to-noise ratio may also exhibit poor consensus if one or two models dominate the response.

3 Midlatitude circulation features: multi-model mean response

This section presents an overview of the multi-model mean circulation response in the 1.5°C experiment (1.5°C−PD) and with an additional 0.5°C of warming (2.0°C−1.5°C). Note that the 1.5°C experiment represents 1.5°C of warming relative to pre-industrial climate, but only 0.7°C of warming compared to the PD. We focus on wintertime (Northern Hemisphere DJF, Southern Hemisphere JJA), when surface baroclinicity is strongest and the midlatitude circulation is most vigorous. This is manifest in a range of atmospheric circulation features (fastest jet streams, highest amplitude stationary waves, storm tracks at maximum intensity), all of which contribute to the large poleward transport of energy during this season (Chang et al., 2002; Trenberth and Stepaniak, 2003). While the winter season is the focus of the study, features of interest in other seasons will be discussed as appropriate. The supplement contains the summer versions of all figures in the section (S2) and the 2.0°C−PD responses (S3).

Generally, circulation changes are quite weak, but somewhat consistent with those observed in the more strongly forced, coupled climate change simulations from CMIP3 and CMIP5 (e.g., Ulbrich et al., 2008; Chang et al., 2012; Simpson et al., 2014; Woollings et al., 2012; Eichler et al., 2013; Barnes and Polvani, 2013). As expected, internal variability is responsible for most of the uncertainty in the responses shown here (Deser et al., 2012; Shepherd, 2014). We first describe the responses of the jet streams, storm tracks and stationary waves, and then draw comparisons with previous studies.

Jet streams. The midlatitude jet stream responses are small and mostly barotropic (observed in $u850$ Fig. 4 and $u250$ Fig. 5), with some differences appearing in the 2.0°C experiment that are not apparent in the 1.5°C response. The main signal is an equatorward shift of the North Pacific jet exit, and a slight poleward shift of the North Pacific jet entrance, consistent with results for RCP8.5 (Simpson et al., 2014). These changes add roughly linearly with the warming from PD to 1.5°C, and from 1.5°C to 2.0°C (compare with Fig. S3.3 and S3.4). In contrast, the North Atlantic jet exhibits different response patterns in 1.5°C−PD and 2.0°C−1.5°C. The 1.5°C experiment shows

Earth Syst. Dynam. Discuss., https://doi.org/10.5194/esd-2017-107
Manuscript under review for journal Earth Syst. Dynam.
Discussion started: 27 November 2017

very little change relative to PD, although the jet entrance shifts slightly equatorward. In the 2.0°C experiment, the jet exit shows a poleward shift and slight extension, associated with a strengthening of low-level westerlies over Europe and a weakening of westerlies over the Mediterranean (Fig. 4). In the Southern Hemisphere, very little response is noted in the 1.5°C experiment other than an extension and slight equatorward shift of the South Pacific jet at upper levels. The 2.0°C−1.5°C response is a strengthening across the South Pacific and a slight poleward shift at upper levels that brings the jet back to its PD position (Fig. S3.3, S3.4).

These experiments do not show the jets clearly migrating or expanding poleward, as found in the more strongly forced CMIP3 (Delcambre et al., 2013) and CMIP5 (Woollings and Blackburn, 2012; Barnes and Polvani, 2013) warming scenarios. The zonal-mean jet shifts are not distinguishable from zero in any season or ocean sector (Fig. 9). In the North Atlantic and Southern Hemisphere, the median jet latitude does show a tendency to shift poleward from 1.5°C to 2.0°C during the shoulder seasons, consistent with the results of Barnes and Polvani (2013). The North Pacific jet exhibits especially large spread, partly related to the longitudinally varying nature of the response (Fig. 4, 5). The winter zonal-mean signal is dominated by the equatorward shift of the jet exit, while the summer zonal-mean signal averages over large and opposing shifts in the jet entrance and exit regions (Fig. 10).

Storm tracks. The storm track responses are also small, but broadly consistent with previous results from CMIP3 and CMIP5 (e.g., Ulbrich et al., 2008; Chang et al., 2012; Zappa et al., 2013). In the Northern Hemisphere, lower level storm activity weakens overall, but the change is generally small except over North America and at very high latitudes (Harvey et al., 2012; Chang, 2013) (Fig. 6). Most of the weakening occurs from PD to 1.5°C; the additional half a degree to 2.0°C does little other than to intensify slightly the tail end of the North Atlantic storm track (compare Fig. 6 and S3.6), consistent with previous studies (e.g., Harvey et al., 2012). In the Southern Hemisphere, lower level storm activity shows weak, patchy changes in the 1.5°C experiment, and still weak but uniform increases in the 2.0°C experiment (see Chang et al., 2012)). The increased storm activity is concentrated on the flanks of the storm track (most apparent in Fig. S3.6), suggesting possible influences on the Antarctic coast to the poleward side, and parts of South America, South Africa and southern Australia to the equatorward side. Upper level storm activity shows a poleward shift and upward expansion of the storm tracks (e.g., Yin, 2005) in both hemispheres, with the response getting larger from 1.5°C to 2.0°C (Fig. 7 and Fig. S3.7). The fact that the upper level responses exhibit similar patterns for 1.5°C−PD and 2.0°C−1.5°C while the lower level responses are quite different supports previous studies suggesting that upper tropospheric eddy activity is less sensitive to local surface forcing (Harvey et al., 2015; Ciasto et al., 2016).

Earth Syst. Dynam. Discuss., https://doi.org/10.5194/esd-2017-107
Manuscript under review for journal Earth Syst. Dynam.
Discussion started: 27 November 2017

Stationary waves. The midlatitude stationary wave response is relatively consistent from the 1.5°C experiment to the 2.0°C experiment (Fig. 8, S3.5). The main feature is over the west coast of North America, where the stationary ridge shifts inland, weakening in southwest and strengthening in northeast. This ridge response enhances southerlies off the west coast and northerlies in the interior of the continent. The response shows good agreement with results from previous studies, which propose changes in the tropics or jet strength as possible mechanisms (Selten et al., 2004; Haarsma and Selten, 2012; Simpson et al., 2016). In the 2.0°C experiment, the ridge response is slightly stronger, while some new (rather small) features emerge at high northern and southern latitudes.

Many of the circulation responses listed above have similar patterns in 2.0°C and 1.5°C, but in some cases, the response patterns change from the initial 0.7° of warming (1.5°C−PD) to the additional 0.5°C of warming (2.0°C−1.5°C). One reason may be that changes in the low-level equator-to-pole temperature contrasts are more important in shaping the 1.5°C response than the 2.0°C response. Greenhouse warming sharpens the upper level temperature gradient and pushes the jet/storm track poleward, while near-surface Arctic amplification of this warming weakens the low-level temperature gradient and pushes the jet/storm track equatorward (e.g., Bengtsson and Hodges, 2006; Brayshaw et al., 2008; Butler et al., 2010; Lu et al., 2010; Graff and LaCasce, 2012; Shaw et al., 2016), with various possibilities for the precise mechanism (Lorenz and DeWeaver, 2007; Chen et al., 2008; Kidston et al., 2011; Michel and Rivière, 2014). The idea that the low-level gradient $\Delta T850$ has greater leverage in the 1.5°C experiment is supported by the fact that it changes less with the additional 0.5°C of warming than with the initial 0.7°C of warming (Fig. 11c for ECHAM6, Table 2 for all models), while the upper level gradient $\Delta T200$ changes more with the additional 0.5°C (Fig. 11a, Table 2). As the world warms, the strengthening upper level gradients should eventually "win", as suggested by the emergence of poleward shifts of the North Atlantic and North Pacific jets in the 2.0°C experiment (Fig. 4, 5). Harvey et al. (2014) found that, in the coupled RCP scenarios, low-level gradient changes are tied to sea ice changes, and upper level gradients changes are tied to tropical SST changes (via the tropical lapse rate). Because sea ice and SST are prescribed in the HAPPI ensemble, there is generally good agreement in the response of these gradients across all models (see Table 3 for the Northern Hemisphere). The exception is the 1.5°C−PD change in $\Delta T200_{\mathrm{NH}}$, possibly due to model-dependence of the tropical lapse rate response.

Another reason for different response patterns in 1.5°C−PD and 2.0°C−1.5°C is simply due to the setup of the experiments. Because aerosols, ozone and land use are kept the same in the 1.5°C and 2.0°C experiments, the influence of these anthropogenic radiative forcings is changing relative to the influence of surface warming. Ozone recovery in particular warms the Antarctic stratosphere during austral summer, opposing the tendency of greenhouse warming to sharpen the upper level gradient $\Delta T200_{\mathrm{SH}}$(Gerber and Son, 2014). The ozone effect dominates the 1.5°C−PD response, but is absent

Earth Syst. Dynam. Discuss., https://doi.org/10.5194/esd-2017-107
Manuscript under review for journal Earth Syst. Dynam.
Discussion started: 27 November 2017

Earth System Dynamics Discussions
Open Access
EGU

in the 2.0°C−1.5°C response, thus accounting for the strong cancellation between 1.5°C−PD and 2.0°C−1.5°C responses in all the summertime circulation features (see supplement S2).

Table 2. Multi-model mean response of equator-to-pole temperature contrast (°C) in winter at 850 hPa and 200 hPa, showing the 5th percentile, median and 95th percentile.

	$\Delta T850_{NH}$	$\Delta T200_{NH}$	$\Delta T850_{SH}$	$\Delta T200_{SH}$
1.5°C−PD				
5%	-1.112	-0.404	-0.450	0.396
median	-0.682	0.745	-0.114	0.894
95%	-0.471	1.320	0.031	1.099
2.0°C−1.5°C				
5%	-0.730	0.031	-0.340	0.492
median	-0.269	1.153	0.040	0.958
95%	-0.066	1.673	0.202	1.173

Table 3. Response of median equator-to-pole temperature contrast (°C) in winter at 850 hPa and 200 hPa.

Model	$\Delta T850_{NH}$		$\Delta T200_{NH}$	
	1.5°C−PD	2.0°C−1.5°C	1.5°C−PD	2.0°C−1.5°C
CAM4	-0.728	-0.240	1.224	1.251
CanAM4	-0.647	-0.398	0.691	1.181
MIROC5	-0.575	-0.242	1.046	1.204
MPI-ECHAM6.3	-0.610	-0.279	0.394	1.092
NorESM1-Happi	-0.676	-0.210	0.591	1.219

4 Case studies

Here, we present case studies to investigate the idea that the documented circulation changes (Fig. 4–8), however weak, may have regional impacts through precipitation (Fig. 2). The cases were selected based on the fact that they show associated changes in circulation and precipitation, yet illustrate that the link between dynamics and impacts under global warming can be different in different locations.

4.1 Mediterranean

The Mediterranean region is thought to be especially vulnerable to drought risk under climate change (Giorgi 2006, Diffenbaugh and Giorgi 2012). Characterized by hot, dry summers, it depends criti-

Earth Syst. Dynam. Discuss., https://doi.org/10.5194/esd-2017-107
Manuscript under review for journal Earth Syst. Dynam.
Discussion started: 27 November 2017

cally on precipitation during the winter season. Under greenhouse warming produced by the RCP scenarios, the region is projected to undergo drying due to a weakening of the Mediterranean storm track (Collins et al., 2013; Zappa et al., 2015a), as measured by reductions in both cyclone activity (Bengtsson et al. 2006; Lionello and Giorgi 2007; Raible et al. 2010) and low-level westerly winds (Zappa et al., 2015b).

In the HAPPI experiments, Mediterranean drying appears to set in somewhere between 1.5°C and 2.0°C of warming according to the multi-model mean (Fig. 12c,d). The drying is a dynamical effect of climate change: weakening of the mean westerlies signals a weakening of the Mediterranean trough seen in the climatological winter zonal wind at 850 hPa ($u850$; contours in Fig. 12a,b for multi-model mean, or in Fig. S1.1 for the separate models and ERA-Interim), which suppresses storm activity. The circulation changes, and hence the dynamical effect, are small in the 1.5°C experiment, thus we do not expect precipitation to change much (Fig. 12a,c). Interestingly, the northern part of the region actually becomes slightly wetter in 1.5°C as part of a general precipitation increase across western Europe (see section 4.2). This is consistent with the idea that, without the dynamical effect, the main influence of climate change would be to increase the amount of precipitation carried by each cyclone, making the region wetter (Zappa et al., 2015a).

Whilst the mean precipitation response in the 2.0°C experiment appears quite clear (Fig. 12c,d), internal variability still plays an important role. Zappa et al. (2015b) previously found a strong, linear relationship between seasonal anomalies in $u850$ and seasonal anomalies in precipitation – a relationship that holds on interannual time scales in observations and historical simulations, as well as on climate change time scales. This $u850$-precipitation relationship also holds across all the models used in this study (Fig. 12e,f). From the scatterplots, it is clear that the responses exhibit considerable spread sampling both positive and negative precipitation changes. In the 1.5°C experiment (Fig. 12e), the distribution straddles zero, making the multi-model mean nearly zero, while in the 2.0°C experiment, the distribution shifts towards more drying (i.e., towards the lower left quadrant of Fig. 12f).

Given the large internal variability, it is perhaps more instructive to examine the distribution of responses rather than the median or mean response. Compositing over the members exhibiting the strongest 5% of wind responses (i.e., most weakening of the westerlies over the Mediterranean box, such that a "strong" response is defined in the sense of the changes in the multi-model mean in Fig. 12d), we see 0.37 mm d^{-1} less precipitation over the region compared to the PD, which represents a reduction of 27% in winter precipitation compared to the PD climatology (Fig. 13a). On the other end of the spectrum, the members with the weakest wind responses actually show slightly more precipitation over the region (0.21 mm d^{-1}; Fig. 13b). Histograms of the changing rainfall distribution for sample locations (Fig. 13c) show a consistent shift towards smaller precipitation rates across most of the region (Rabat, Morocco and Athens, Greece), despite very weak changes in the mean/median precipitation values (Table 4). Lisbon, Portugal, which is situated in the northern part

Earth Syst. Dynam. Discuss., https://doi.org/10.5194/esd-2017-107
Manuscript under review for journal Earth Syst. Dynam.
Discussion started: 27 November 2017

Earth System Dynamics
Discussions
Open Access
EGU

of the region, exhibits a shift towards slightly wetter winters in the 1.5°C experiment before the drying sets in at 2.0°C.

Table 4. Precipitation (mm d^{-1}) for sample locations from the CAM4 ensemble, consistent with the histograms in Fig. 13c.

	Experiment			
	PD	1.5°C	2.0°C	
Athens,	2.102	2.069	2.000	mean
Greece	2.105	2.065	1.997	median
	1.775	1.718	1.651	5%
	2.433	2.437	2.395	95%
Lisbon,	1.475	1.501	1.342	mean
Portugal	1.461	1.497	1.333	median
	1.106	1.122	0.979	5%
	1.918	1.955	1.751	95%
Rabat,	0.545	0.521	0.421	mean
Morocco	0.536	0.511	0.412	median
	0.355	0.334	0.254	5%
	0.743	0.750	0.603	95%

The signal beginning to emerge in a 2.0°C world is effectively a poleward expansion of climate zones accompanying a poleward expansion of the Hadley cell (Lu et al., 2007). The Köppen-Geiger scheme for climate zones (Fig. 13d) classifies the Mediterranean today as a temperate region (Csa, Csb; characterized by dry summers), containing some arid steppe microclimates (BSk, BSh). Under global warming, the North African arid belt pushes northwards, and the Mediterranean temperate zone spreads into Europe. Places that may be most susceptible to winter rainfall deficits are those situated where the drying is most pronounced (e.g., see Iberian Peninsula in Fig. 13a and Lisbon responses in Fig. 13c, Table 4) or near the transition to the Sahara Desert (e.g., see Rabat responses).

4.2 Euro-Atlantic region

The atmospheric circulation response to climate change in the Euro-Atlantic sector exhibits substantial uncertainty due to large internal variability and the influence of Arctic amplification, which is pronounced in the region. In CMIP scenarios with midrange to strong warming, previous studies have noted an eastward extension of the winter storm track into Europe, with higher cyclone frequencies in central Europe and reduced cyclone frequencies in Scandinavia and the Mediterranean (Chang et al., 2012; Harvey et al., 2012; Zappa et al., 2013). These storm track changes are associ-

Earth Syst. Dynam. Discuss., https://doi.org/10.5194/esd-2017-107
Manuscript under review for journal Earth Syst. Dynam.
Discussion started: 27 November 2017

ated with a robust poleward shift of the North Atlantic jet, primarily in the exit region, in all seasons except winter, even in the most strongly forced RCP8.5 scenario (Woollings and Blackburn, 2012; Barnes and Polvani, 2013).

In the HAPPI experiments, there are signs that similar changes are emerging, although in some cases not until 2.0°C warming. The North Atlantic jet exit shifts poleward in the 2.0°C experiment (Fig. 4, 5). In the 1.5°C experiment, near-surface Arctic amplification has considerable leverage (as noted in the discussion surrounding Fig. 11), resulting in a slight equatorward shift of the jet entrance. At low levels, the multi-model mean exhibits stronger westerlies over the continent in both warming experiments, with weaker westerlies over the Mediterranean in the 2.0°C experiment (Fig. 12a,b). Finally, the storm track exit is slightly enhanced at 1.5°C and extends eastward into Europe at 2.0°C, with considerable spread due to internal variability (Fig. 14a,b).

These circulation changes are tied to precipitation impacts over Europe, but in contrast to the Mediterranean, they reinforce (rather than oppose) the thermodynamic effect. Western Europe has reliable, year-round precipitation and sees increasing precipitation with warming (Fig. 12c,d), evident in both the 1.5°C and 2.0°C experiments. This is partly due to the thermodynamic increase in tropospheric moisture content, which alters moisture fluxes and leads to wet regions getting wetter (Held and Soden, 2006). On top of this, the dynamic effect (extension of the storm track in 2.0°C) also contributes to wetting the region (Fig. 14a,b). The signal-to-noise ratio of the storm track response is small, reflecting the tendency of models to place the climatological storm track in slightly different locations (Fig. S1.5). Figure 14c shows that the increase in mean precipitation with warming is comparable for 2.0°C−1.5°C and 1.5°C−PD, while the 95th percentile limit shifts more for 2.0°C−1.5°C than 1.5°C−PD.

Finally, the mean sea level pressure (MSLP) responses are also small, but consistent with the jet changes (Fig. 15). The 1.5°C experiment shows a negative anomaly in the eastern Atlantic where we note an equatorward shift of the jet entrance (Fig. 15a). There is a slight increase over Iceland increases and a slight decrease over the Azores, suggesting lower values of the North Atlantic Oscillation (NAO) index. The 2.0°C experiment shows a dipole over the European sector (negative anomalies over Scandinavia, positive over the Mediterranean) consistent with a poleward shift of the jet exit (Fig. 15b). However, the response over the NAO centres of action is very weak (see stippling). We calculate a daily wintertime (DJF) NAO index for each ensemble member by subtracting the standardized SLP at Reykjavik from the standardized SLP at the Azores (the standardization uses the multi-model PD ensemble as the reference time series). The daily NAO index is averaged over each member to produce a distribution of decadal NAO variability for each model (Fig. 15c). The changes in the NAO are model-dependent, but a robust feature is a shift towards more negative NAO values in the 1.5°C experiment (equatorward shift of jet exit) and a slight shift back towards more positive NAO values in 2.0°C−1.5°C (poleward shift of the jet entrance).

Earth Syst. Dynam. Discuss., https://doi.org/10.5194/esd-2017-107
Manuscript under review for journal Earth Syst. Dynam.
Discussion started: 27 November 2017

4.3 North American west coast

The North American west coast is the last case study, chosen to illustrate the different effects that circulation changes may have on precipitation at different locations. In the strong warming RCP8.5 scenario, models project a drying of the interior southwest of the continent and a wetting to the north (including the west coast from California up to Alaska) during the winter half-year due primarily to changes in moisture convergence associated with the mean flow (Seager et al., 2014). Two notable features appear in the multi-model mean circulation response over the region: (1) an extension and equatorward shift of the North Pacific jet exit that enhance westerlies just offshore of the west coast (seen in the $u250$ field in Fig. 5), and (2) an inland migration of the North American ridge that enhances southerlies into Alaska (Fig 8; see also Selten et al. (2004); Haarsma and Selten (2012); Simpson et al. (2016)). We examine the relationship between these wind changes and precipitation at two locations along the west coast. Because 2.0°C of warming produces changes that are similar to, but larger than, those with 1.5°C of warming, only the 2.0°C results are shown here.

On the central west coast, the jet ($u250$) and stationary ridge ($v250*$) changes appear to have competing (or at least offsetting) effects on precipitation. In members with the strongest $u850$ response (most positive westerly anomaly offshore), the region becomes wetter (southern pink box in Fig. 16a) along with a slight enhancement of low-level storm activity just offshore (Fig. S3.6a,c). In members with the strongest $v250*$ response (inland ridge shift), there is little change to slight wetting (Fig. 16c). Precipitation signals associated with jet changes are larger than those associated with ridge changes. Within the spread produced by internal variability, the jet response can be positive or negative, such that the members with the weakest $u250$ responses yield show drying along the central west coast (Fig. 16b).

On the southern coast of Alaska (northern pink box in Fig 16a), both the jet and stationary ridge changes are associated with increased precipitation. However, it is a strong $v250*$ response that produces the most wetting (Fig. 16b), consistent with the relationship between stronger offshore southerlies and a wetting of northwestern North America (Seager et al., 2014). Internal variability, while still present, is not important to the overall sign of the precipitation response: members at the other end of the spectrum still become wetter in the region, although only very slightly (Fig.16d).

5 Discussion and concluding remarks

This study presents an overview of the global midlatitude circulation response to 1.5°C and 2.0°C of warming compared to pre-industrial conditions using the HAPPI ensemble. The main findings are as follows:

- The large ensembles reveal complex responses to the HAPPI forcings, with internal (decadal) variability playing an important role in the ensemble spread.

Earth Syst. Dynam. Discuss., https://doi.org/10.5194/esd-2017-107
Manuscript under review for journal Earth Syst. Dynam.
Discussion started: 27 November 2017

- In the 1.5°C experiment, there is a weakening of storm activity over North America, an inland shift of the North American stationary ridge, an equatorward shift of the North Pacific jet exit, and an equatorward intensification of the South Pacific jet. With an additional 0.5°C of warming, most response features are enhanced but some new ones emerge, most notably a poleward shift of the North Atlantic jet exit, an eastward extension of the North Atlantic storm track into Europe, and an intensification on the flanks of the Southern Hemisphere storm track.

- Mediterranean: The projected drying of the region emerges in the 2.0°C world, along with a weakening of the Mediterranean storm track. Even with 2.0°C of warming, however, the ensemble spread allows for both increased and decreased precipitation responses.

- Western Europe: The region becomes increasingly wet from 1.5°C to 2.0°C, although the main circulation changes (slight poleward shift in the North Atlantic jet and eastward extension of the low-level storm track) only appear in the 2.0°C experiment.

- North American west coast: This region gets wetter with warming, mainly due to the inland shift of the North American stationary ridge, but the main circulation changes have slight differently influences on precipitation in different locations.

While the unique experimental design of the HAPPI ensemble is an advantage, it also introduces limitations that must be considered when interpreting and applying our results. The specified SST and sea ice conditions allow for large ensembles, but there is high uncertainty on future SST and sea ice changes. At least by constructing the forcings as an ensemble mean over all CMIP5 models, potential errors in these fields are likely smaller than errors from an individual model. But local features of the forcing seem to heavily influence the regional changes in these low-end warming scenarios, as evidenced by the complex, nonlinear behaviour in the 1.5°C−PD and 2.0°C−1.5°C responses. Furthermore, the single realization of SST and sea ice patterns as well as the lack of atmosphere-ocean-ice coupling offer a restricted view of ocean-driven variability and internal variability, which is sure to influence the simulated climate variability. Comparisons with related coupled experiments (e.g., Sanderson et al., 2017; Iversen et al., submitted 2017) would be a useful exercise for evaluating whether coupling changes the results presented here.

There remain many interesting large-scale questions to explore using the HAPPI ensemble, including deeper investigations of how individual model biases affect the responses and their spread; focus studies on particular regions where the additional half a degree of warming yields impacts not seen in the 1.5°C experiment; and potential consequences of uncertainties in future SST and sea ice changes.

Acknowledgements. CM and LSG contributed equally to the study. This work was supported by the Norwegian Research Council projects no. 261821 HappiEVA (IB, LSG, TI, CM), no. 231716 jetSTREAM (CM), no.

255027 DynAMiTe (MPK); the U.S. Department of Energy, Office of Science, Office of Biological and Environmental Research contract DE-AC02-05CH11231 (HK, DAS); funding from the Bundesministerium für Bildung und Forschung BMBF (LL). We also acknowledge the Norwegian Metacenter for Computational Science and Storage Infrastructure (NOTUR and Norstore Projects NN2345k and NS2345k); and the European Centre for Medium-Range Weather Forecasts for providing the ERA-Interim data. Finally, we thank M. Esch, K.-H. Wieners, S. Hagemann, T. Mauritsen from MPI-M for technical support with ECHAM6.3; and S. Legutke, E. Madonna, S. Sobolowski for helpful discussions.

Earth Syst. Dynam. Discuss., https://doi.org/10.5194/esd-2017-107
Manuscript under review for journal Earth Syst. Dynam.
Discussion started: 27 November 2017

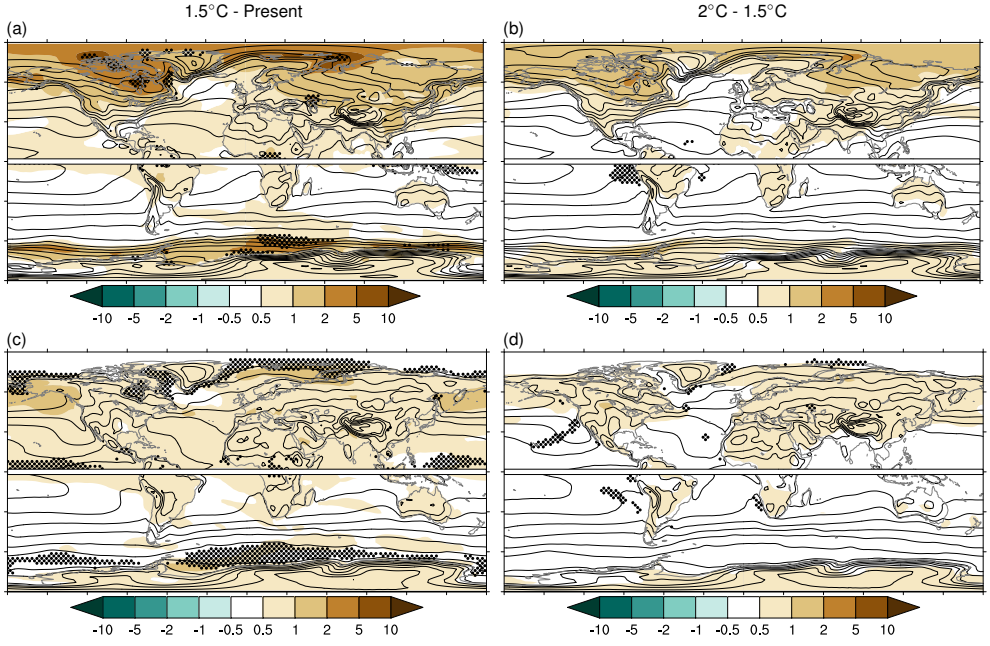

Figure 1. Multi-model mean response of surface air temperature for 1.5°C−PD (left) and 2.0°C−1.5°C (right). Top panels show winter (Northern Hemisphere DJF, Southern Hemisphere JJA) responses (shading; units K) along with the climatology (contour interval 5 K) for the (a) PD and (b) 1.5°C experiments. Bottom panels show the same for summer (Northern Hemisphere JJA, Southern Hemisphere DJF). Black dots mask out regions where model consensus is low ($f^2 > 1$) on the magnitude of the response (see section 2.2 for details).

Earth Syst. Dynam. Discuss., https://doi.org/10.5194/esd-2017-107
Manuscript under review for journal Earth Syst. Dynam.
Discussion started: 27 November 2017

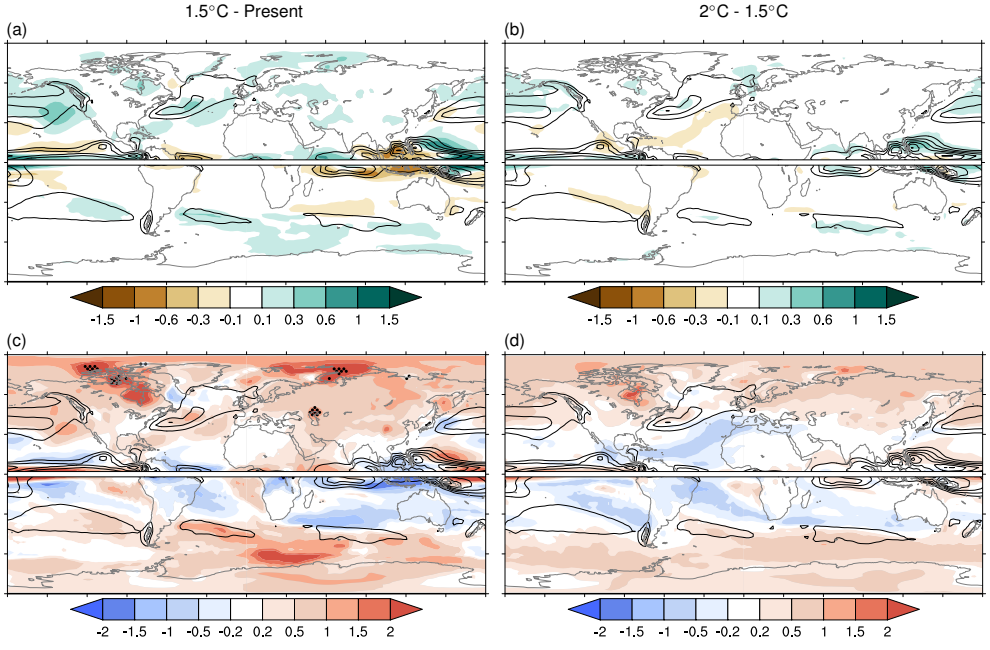

Figure 2. Multi-model mean esponse of winter (Northern Hemisphere DJF, Southern Hemisphere JJA) precipitation for 1.5°C−PD (left) and 2.0°C−1.5°C (right). Top panels show responses (shading; units mm d^{-1}) along with the climatology (contour interval 2 mm d^{-1} starting from 4 mm d^{-1}) for the (a) PD and (b) 1.5°C experiments. Bottom panels show signal-to-noise ratio β/σ, where the sign corresponds to the sign of the response. In (c) and (d), black dots mask out regions where consensus is low ($f^2 > 1$) on the magnitude of the response.

Earth Syst. Dynam. Discuss., https://doi.org/10.5194/esd-2017-107
Manuscript under review for journal Earth Syst. Dynam.
Discussion started: 27 November 2017

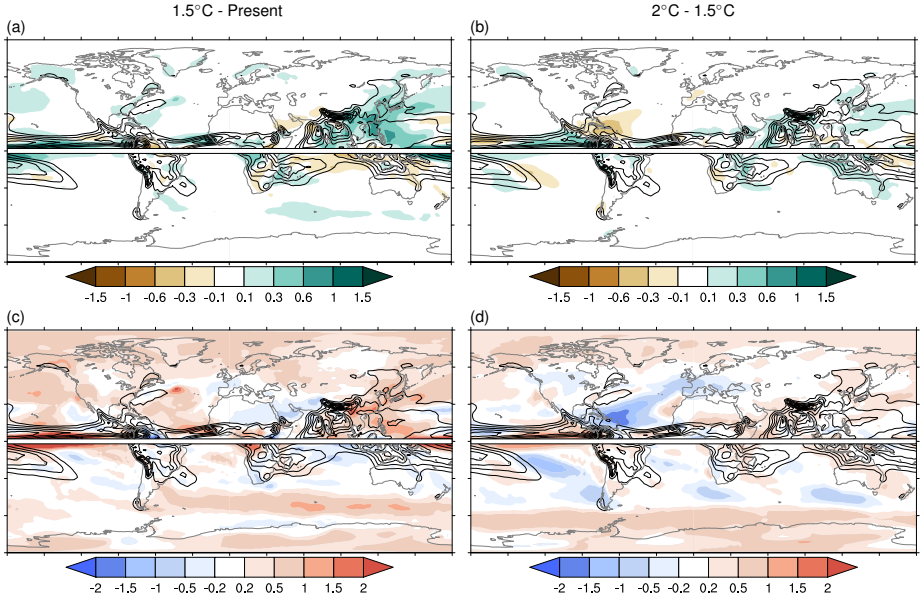

Figure 3. As in Figure 3 but for summer (Northern Hemisphere JJA, Southern Hemisphere DJF) precipitation.

Earth Syst. Dynam. Discuss., https://doi.org/10.5194/esd-2017-107
Manuscript under review for journal Earth Syst. Dynam.
Discussion started: 27 November 2017

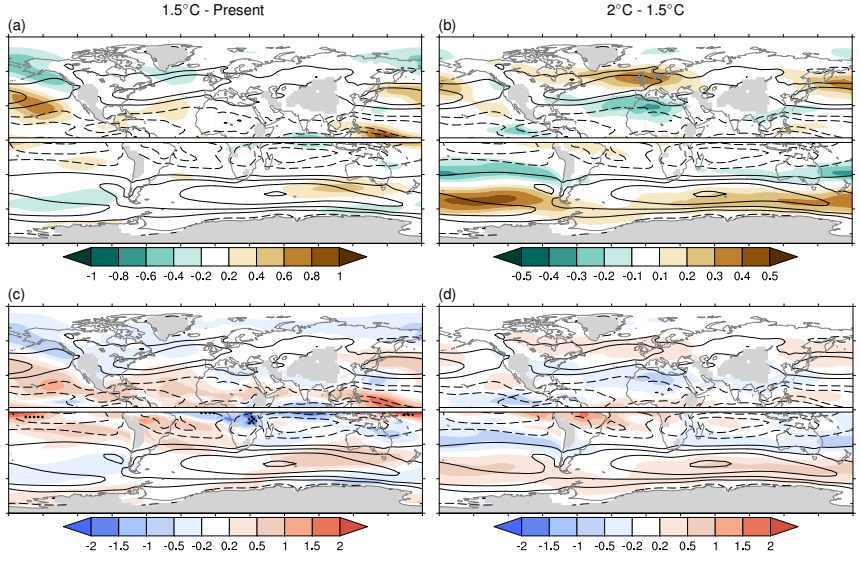

Figure 4. Multi-model mean response of winter (Northern Hemisphere DJF, Southern Hemisphere JJA) zonal wind at 850 hPa ($u850$) for 1.5°C−PD (left) and 2.0°C−1.5°C (right). Top panels show responses (shading; units m s^{-1}) along with the climatology (contour interval 4 m s^{-1}) for the (a) PD and (b) 1.5°C experiments. Note the different colour scale for (a) and (b). Bottom panels show signal-to-noise ratio β/σ, where the sign corresponds to the sign of the response. In (c) and (d), black dots (if present) mask out regions where consensus is low ($f^2 > 1$) on the magnitude of the response; grey shading indicates regions of high topography intersecting the plotted variable.

Earth Syst. Dynam. Discuss., https://doi.org/10.5194/esd-2017-107
Manuscript under review for journal Earth Syst. Dynam.
Discussion started: 27 November 2017

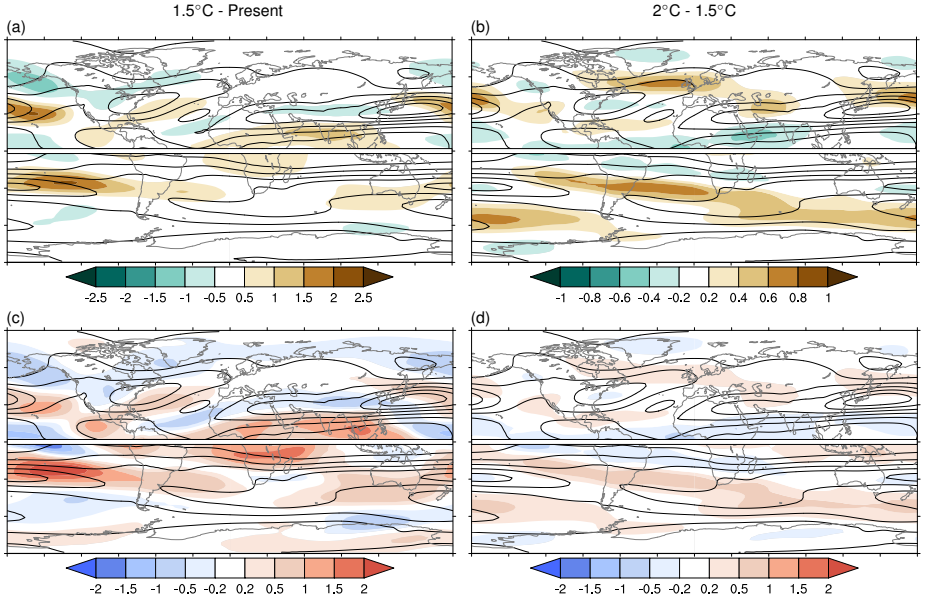

Figure 5. Multi-model mean response of winter (Northern Hemisphere DJF, Southern Hemisphere JJA) zonal wind at 250 hPa ($u250$) for 1.5°C−PD (left) and 2.0°C−1.5°C (right). Top panels show responses (shading; units m s^{-1}) along with the climatology (contour interval 10 m s^{-1}) for the (a) PD and (b) 1.5°C experiments. Note the different colour scale for (a) and (b). Bottom panels show signal-to-noise ratio β/σ, where the sign corresponds to the sign of the response. In (c) and (d), black dots (if present) mask out regions where consensus is low ($f^2 > 1$) on the magnitude of the response.

Earth Syst. Dynam. Discuss., https://doi.org/10.5194/esd-2017-107
Manuscript under review for journal Earth Syst. Dynam.
Discussion started: 27 November 2017

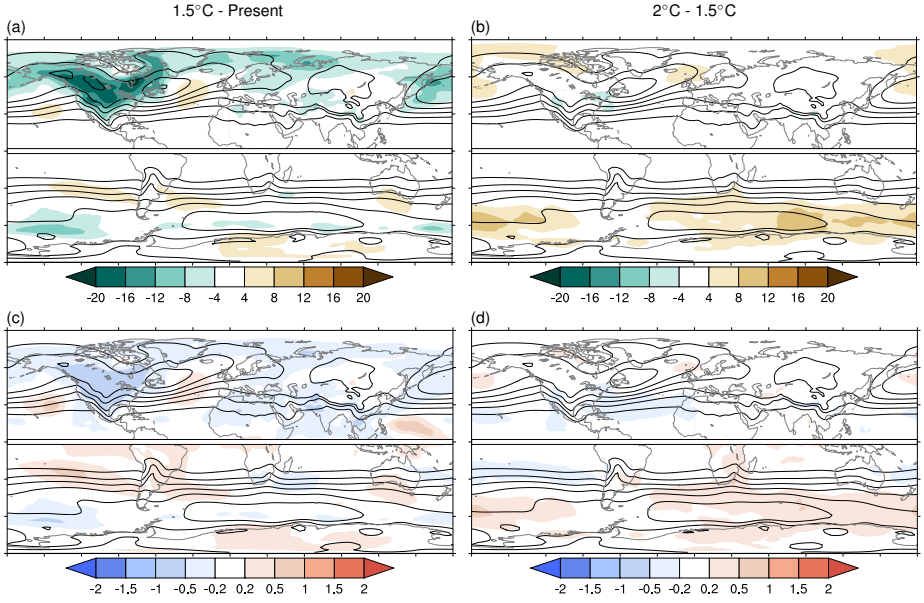

Figure 6. Multi-model mean response of winter (Northern Hemisphere DJF, Southern Hemisphere JJA) low-level MSLP storm tracks for 1.5°C−PD (left) and 2.0°C−1.5°C (right). Top panels show responses (shading; units hPa) along with the climatology (contour interval 100 hPa) for the (a) PD and (b) 1.5°C experiments. Bottom panels show signal-to-noise ratio β/σ, where the sign corresponds to the sign of the response. In (c) and (d), black dots (if present) mask out regions where consensus is low ($f^2 > 1$) on the magnitude of the response. The storm tracks are defined as the standard deviation of bandpass filtered daily MSLP.

Earth Syst. Dynam. Discuss., https://doi.org/10.5194/esd-2017-107
Manuscript under review for journal Earth Syst. Dynam.
Discussion started: 27 November 2017

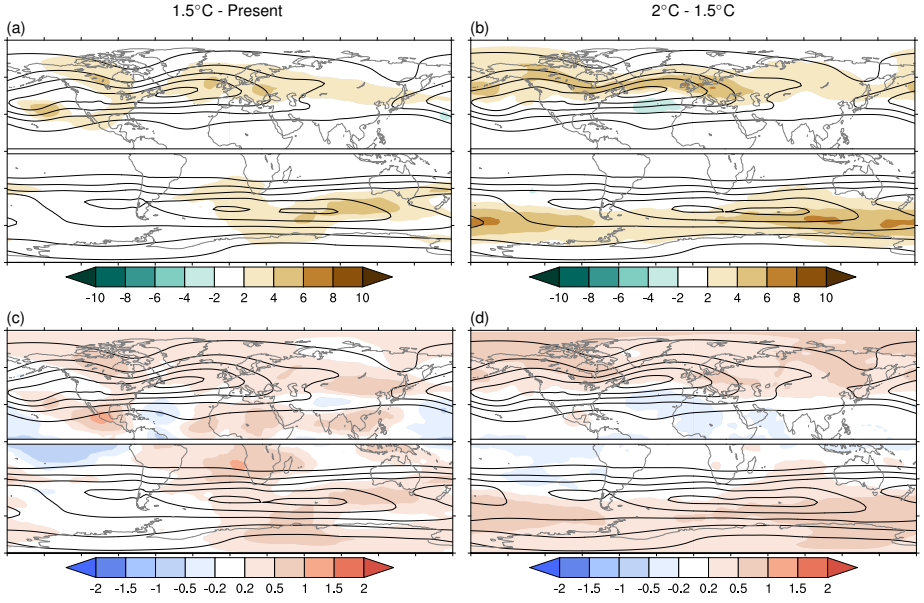

Figure 7. Multi-model mean response of winter (Northern Hemisphere DJF, Southern Hemisphere JJA) upper level EKE storm tracks for 1.5°C−PD (left) and 2.0°C−1.5°C (right). Top panels show responses (shading; units $m^2\ s^{-2}$) along with the climatology (contour interval 40 $m^2\ s^{-2}$) for the (a) PD and (b) 1.5°C experiments. Bottom panels show signal-to-noise ratio β/σ, where the sign corresponds to the sign of the response. In (c) and (d), black dots (if present) mask out regions where consensus is low ($f^2 > 1$) on the magnitude of the response. The storm tracks are defined as bandpass filtered daily EKE at 250 hPa.

Earth Syst. Dynam. Discuss., https://doi.org/10.5194/esd-2017-107
Manuscript under review for journal Earth Syst. Dynam.
Discussion started: 27 November 2017

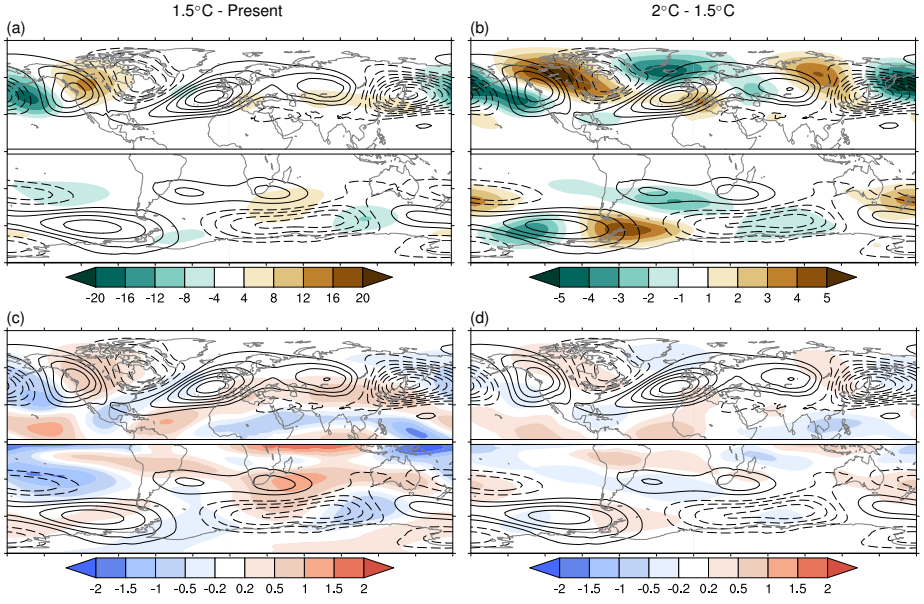

Figure 8. Multi-model mean response of winter (Northern Hemisphere DJF, Southern Hemisphere JJA) stationary waves at 500 hPa for 1.5°C−PD (left) and 2.0°C−1.5°C (right). Top panels show responses (shading; units m) along with the climatology (contour interval 25 m) for the (a) PD and (b) 1.5°C experiments. Note the different colour scale for (a) and (b). Bottom panels show signal-to-noise ratio β/σ, where the sign corresponds to the sign of the response. In (c) and (d), black dots (if present) mask out regions where consensus is low ($f^2 > 1$) on the magnitude of the response. Stationary waves are defined as departures from the zonal mean of geopotential height (Z^*) at 500 hPa.

Earth Syst. Dynam. Discuss., https://doi.org/10.5194/esd-2017-107
Manuscript under review for journal Earth Syst. Dynam.
Discussion started: 27 November 2017

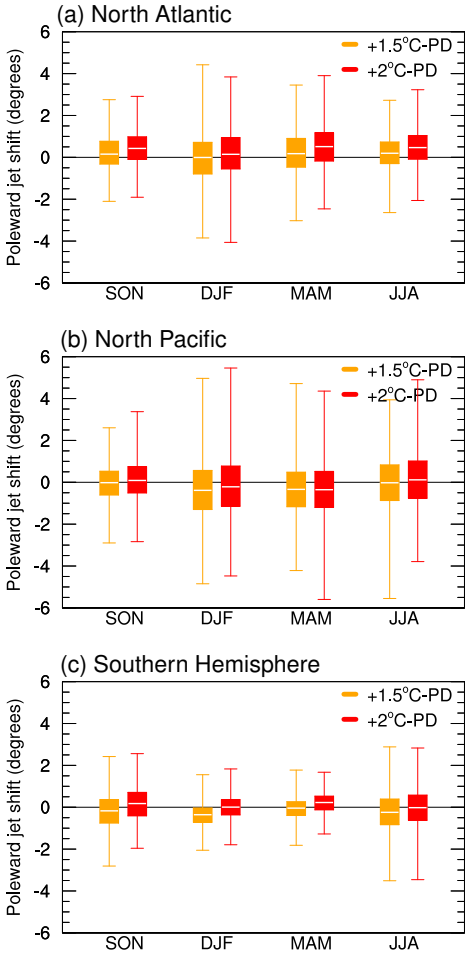

Figure 9. Multi-model mean shift of the eddy-driven jet in the PD (grey), 1.5°C (orange) and 2.0°C (red) experiments for each season. The white horizontal line in the boxes indicates the median, the boxes indicate the interquartile range, and the whiskers indicate the full ensemble spread. The jet latitude was determined according to the method of Woollings et al. (2010).

Earth Syst. Dynam. Discuss., https://doi.org/10.5194/esd-2017-107
Manuscript under review for journal Earth Syst. Dynam.
Discussion started: 27 November 2017

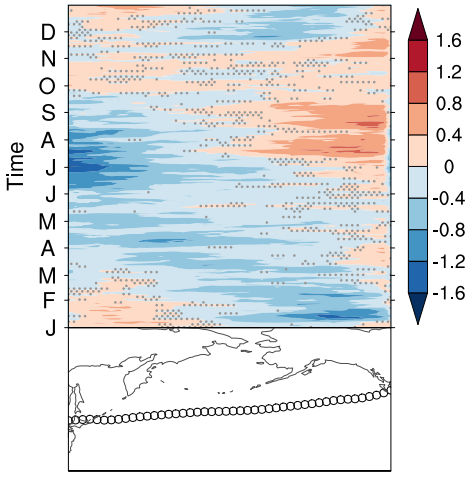

Figure 10. Multi-model mean shift of the winter North Pacific eddy-driven jet (shading, in degrees latitude) in the 2.0°C experiment compared to the PD experiment. Dots mask out places where fewer than three of five models simulate the same response sign as the multi-model mean. The bottom panel shows the climatological position of the jet in the PD experiment.The jet latitude was determined according to the method of Woollings et al. (2010).

Earth Syst. Dynam. Discuss., https://doi.org/10.5194/esd-2017-107
Manuscript under review for journal Earth Syst. Dynam.
Discussion started: 27 November 2017

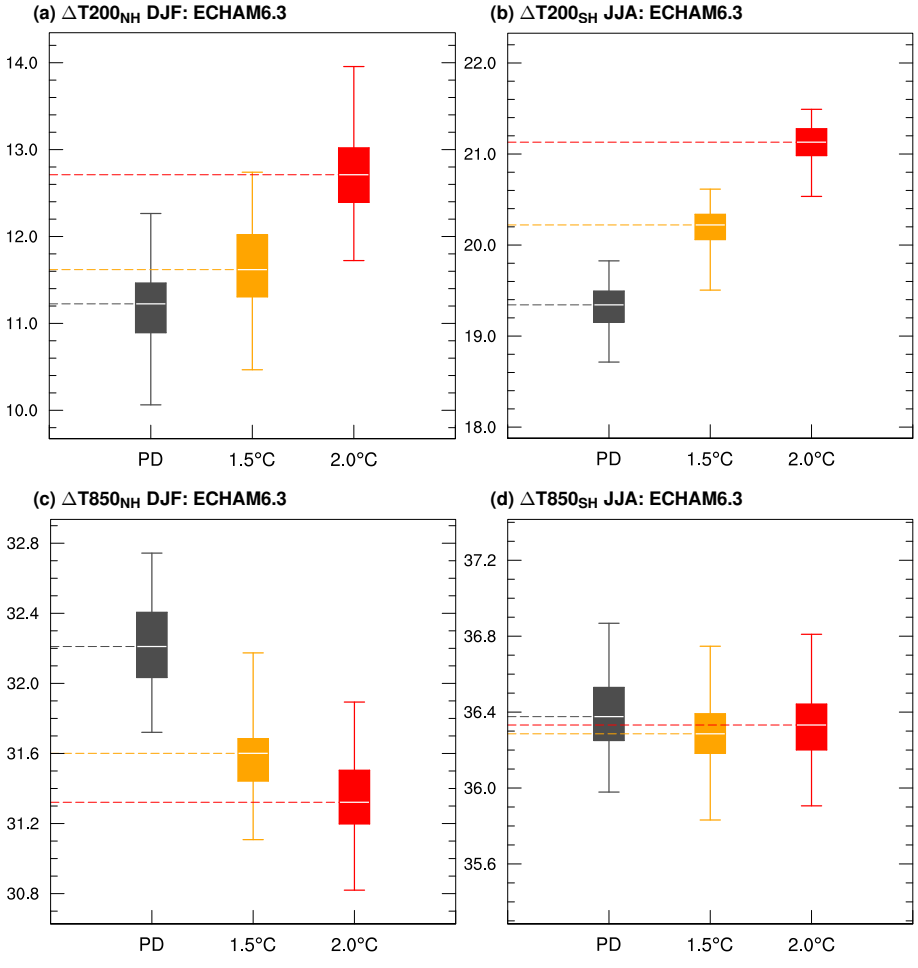

Figure 11. Changes in upper and lower level equator-to-pole temperature gradients (following Harvey et al., 2014) in the PD (grey), 1.5°C (orange) and 2.0°C (red) experiments in the ECHAM6 ensemble. The Northern Hemisphere temperature gradient is defined as the difference between the area-averaged temperature in the 30°S–30°N band and the region poleward of 60°N, taken at 850 hPa ($\Delta T850_{\mathrm{NH}}$) and 200 hPa ($\Delta T200_{\mathrm{NH}}$). The Southern Hemisphere gradient is defined as the the difference between the 30°S–30°N band and the region poleward of 60°S, taken at 850 hPa ($\Delta T850_{\mathrm{SH}}$) and 200 hPa ($\Delta T200_{\mathrm{SH}}$). The white horizontal line in the boxes indicates the median, the boxes indicate the interquartile range, and the whiskers indicate the ECHAM6 ensemble spread. Dashed horizontal lines mark the changes in the median between the experiments.

Earth Syst. Dynam. Discuss., https://doi.org/10.5194/esd-2017-107
Manuscript under review for journal Earth Syst. Dynam.
Discussion started: 27 November 2017

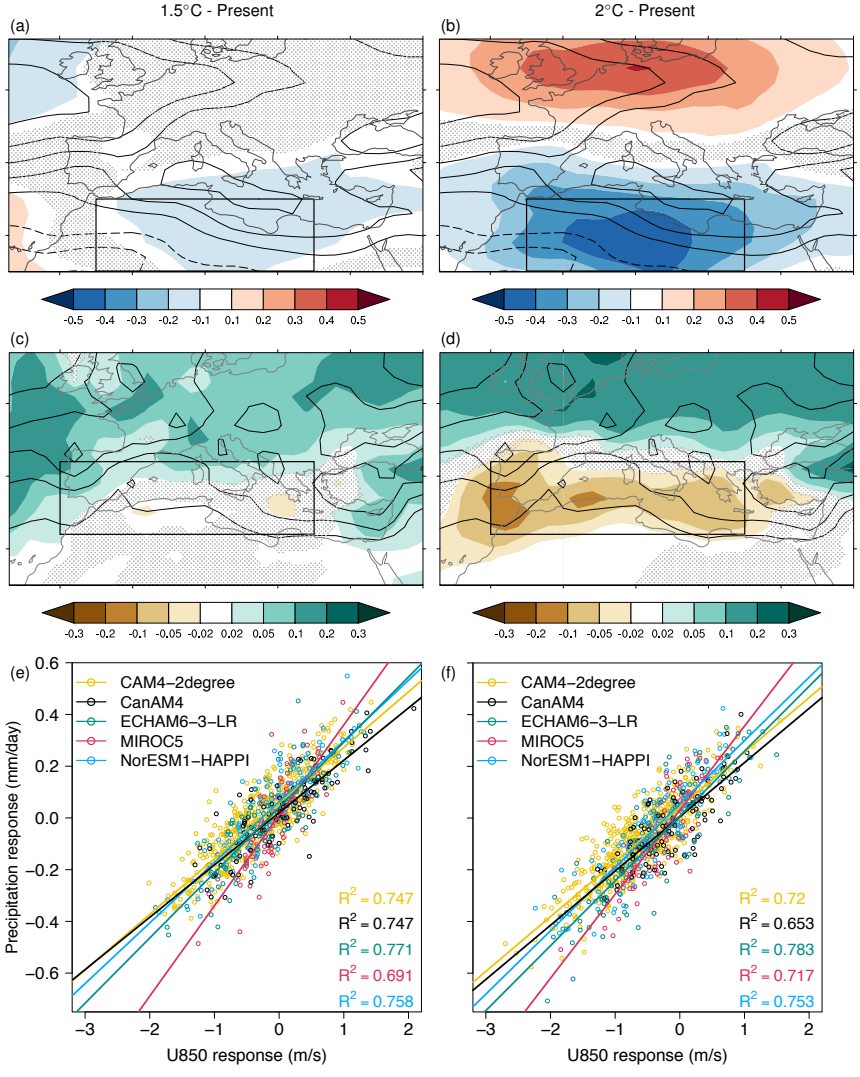

Figure 12. Multi-model mean winter (DJF) response of (a-b) zonal wind at 850 hPa and (c-d) precipitation in the 1.5°C (left) and 2.0°C (right) experiments relative to PD. Top panels show the multi-model mean responses (shading) and the PD climatology (contour interval 2 m s^{-1}, dashed contours for negative values, zero contour omitted) for $u850$. Middle panels show the multi-model mean responses (shading) and the PD climatology (contour interval 1 mm d^{-1}) for precipitation. Stippling in (a) to (d) masks out regions where the response is very weak (signal-to-noise ratio $|\beta/\sigma| < 0.1$). Bottom panels show the relationship between the area-averaged precipitation and $u850$ responses in the (e) 1.5°C and (f) 2.0°C experiments relative to PD. Boxes in the maps indicate the regions used for calculating area-averaged responses.

Earth Syst. Dynam. Discuss., https://doi.org/10.5194/esd-2017-107
Manuscript under review for journal Earth Syst. Dynam.
Discussion started: 27 November 2017

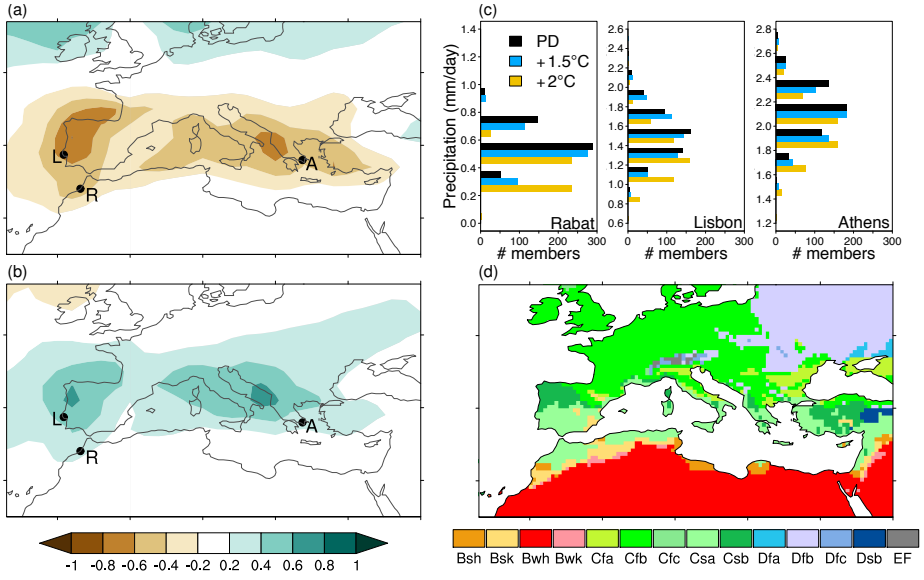

Figure 13. Spread in projected winter (DJF) precipitation changes for the Mediterranean. Composites of precipitation anomalies (mm d^{-1}) over the members with the (a) strongest 5% and (b) weakest 5% of u850 responses within each model ensemble in the 2.0°C experiment. A strong u850 response is defined in the sense of the multi-model mean in Fig. 12. (c) Histograms of precipitation in Rabat, Lisbon and Athens for the PD, 1.5°C and 2.0°C experiments from the CAM4 ensemble. The locations are indicated in the maps. (d) Climate zones according to the Köppen-Geiger classification scheme (Kottek et al., 2006). The Mediterranean is primarily a temperate zone with dry summers (Csa, Csb), but includes some arid regions (BSk, BSh).

Earth Syst. Dynam. Discuss., https://doi.org/10.5194/esd-2017-107
Manuscript under review for journal Earth Syst. Dynam.
Discussion started: 27 November 2017

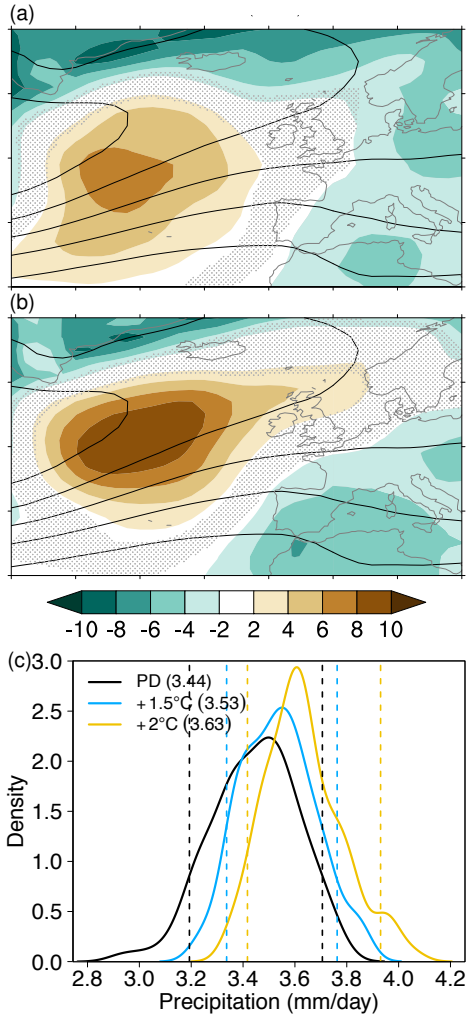

Figure 14. Multi-mean model response of the winter (DJF) low-level MSLP storm track in (a) 1.5°C and (b) 2.0°C relative to PD (shading, units: Pa) along with the PD climatology (contour interval 100 Pa) over the Euro-Atlantic sector. Stippling masks out regions where the response is very weak (signal-to-noise ratio $|\beta/\sigma| < 0.1$). (c) Distribution of area-averaged precipitation over northwestern Europe (45°N–60°N / 10°W–10°E) for the PD, 1.5°C and 2.0°C experiments in the CanAM4 ensemble (solid lines). The dashed lines represent the 5th and 95th percentiles of each distribution; mean values for each experiment are indicated in the legend.

Earth Syst. Dynam. Discuss., https://doi.org/10.5194/esd-2017-107
Manuscript under review for journal Earth Syst. Dynam.
Discussion started: 27 November 2017

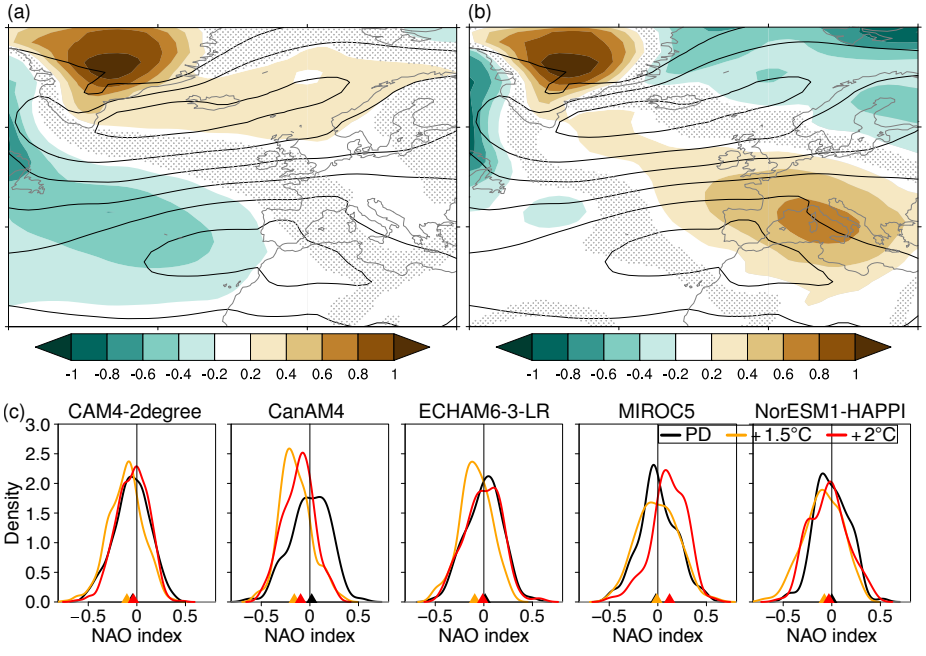

Figure 15. Multi-model response of winter (DJF) sea level pressure over the Euro-Atlantic sector in (a) 1.5°C and (b) 2.0°C relative to PD (shading, units: hPa) along with the PD climatology (contour interval 5 hPa). (c) Distributions of the NAO index showing the spread and median (triangle) for each model and experiment.

Earth Syst. Dynam. Discuss., https://doi.org/10.5194/esd-2017-107
Manuscript under review for journal Earth Syst. Dynam.
Discussion started: 27 November 2017

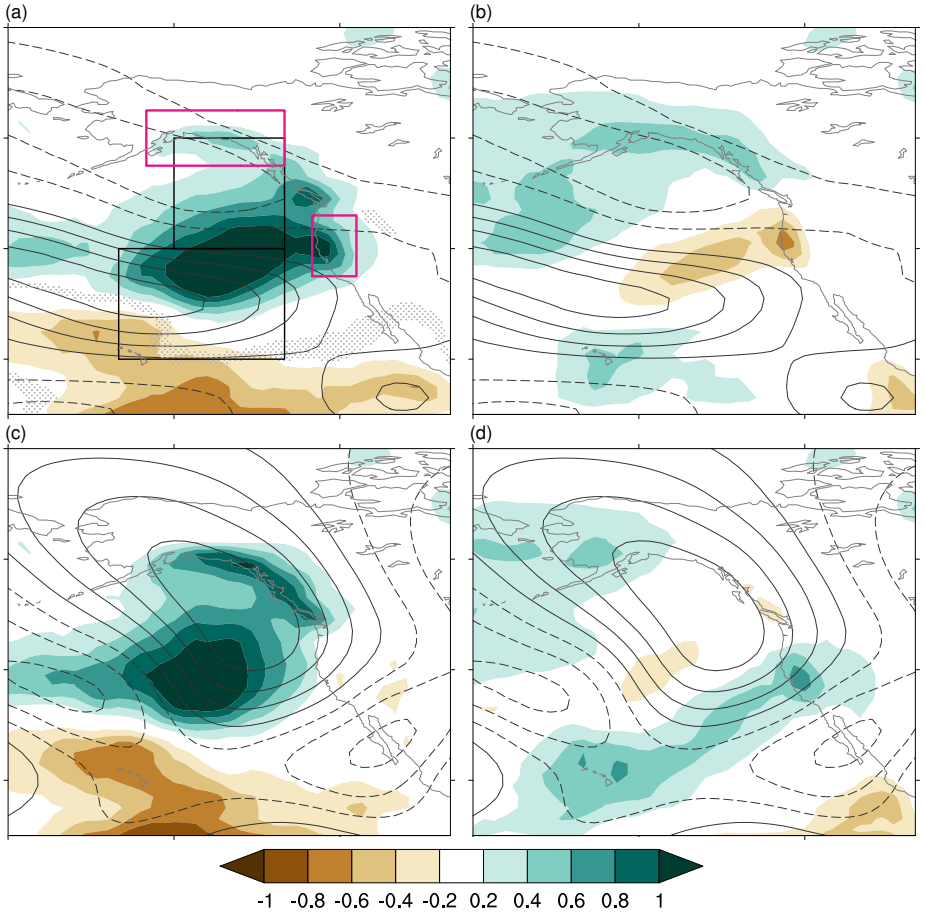

Figure 16. Precipitation signals associated with wind changes over western North America in the 2.0°C experiment. Top: Composites of precipitation based on westerly $u250$ changes in the North Pacific jet exit (area indicated in (a) by southern black box), over members with the (a) 5% strongest and (b) 5% weakest westerly responses. Contours show the $u250$ climatology (contour interval 0.5 m s^{-1}, zero contour omitted) for the PD experiment. Bottom: Composites of precipitation based on southerly $v250*$ changes off the coast (area indicated in (a) by northern black box, over members with the (c) 5% strongest and (d) 5% weakest southerly responses. Contours show the $v250*$ climatology (contour interval 0.4 m s^{-1}, zero contour omitted) for the PD experiment, where $v250*$ is the departure from the zonal mean of the meridional wind at 250 hPa. These composites use data from the five models.

Earth Syst. Dynam. Discuss., https://doi.org/10.5194/esd-2017-107
Manuscript under review for journal Earth Syst. Dynam.
Discussion started: 27 November 2017

References

United Nations Framework Convention on Climate Change (UN-FCCC): Adoption of the Paris Agreement, 2015.

Baker, H.: The impact of CO_2 concentration at 1.5°C global warming on climate extremes, Nature, in review 2017.

Barnes, E. A. and Polvani, L.: Response of the midlatitude jets, and of their variability, to increased greenhouse gases in the CMIP5 models, J. Clim., 26, 7117–7135, doi:10.1175/ JCLI-D-12-00536.1, 2013.

Bengtsson, L. and Hodges, K. I.: Storm tracks and climate change, J. Clim., 19, 3518–3543, 2006.

Bentsen, M., Bethke, I., Debernard, J. B., Iversen, T., Kirkevåg, A., Seland, Ø., Drange, H., Roelandt, C., Seierstad, I. A., Hoose, C., and Kristjánsson, J. E.: The Norwegian Earth System Model, NorESM1-M Part 1: Description and basic evaluation of the physical climate, Geoscientific Model Development, 6, 687–720, doi:10.5194/gmd-6-687-2013, https://www.geosci-model-dev.net/6/687/2013/, 2013.

Brayshaw, D. J., Hoskins, B., and Blackburn, M.: The Storm-Track Response to Idealized SST Perturbations in an Aquaplanet GCM, J. Atmos. Sci., 65, 2842–2860, doi:10.1175/2008JAS2657.1, 2008.

Butler, A. H., Thompson, D. W. J., and Heikes, R.: The Steady-State Atmospheric Circulation Response to Climate Change-like Thermal Forcings in a Simple General Circulation Model, J. Clim., 23, 3474–3496, doi:10.1175/2010JCLI3228.1, 2010.

Chang, E. K. M.: CMIP5 Projection of Significant Reduction in Extratropical Cyclone Activity over North America, J. Clim., 26, 9903–9922, 2013.

Chang, E. K. M., Lee, S., and Swanson, K. L.: Storm Track Dynamics, J. Clim., 15, 2163–2183, doi:10.1175/1520-0442(2002)015<02163:STD>2.0.CO;2, 2002.

Chang, E. K. M., Guo, Y., and Xia, X.: CMIP5 multimodel ensemble projection of storm track change under global warming, J. Geophys. Res., 117, D23 118, doi:10.1029/2012JD017816, 2012.

Chen, G., Lu, J., and Frierson, D. M. W.: Phase Speed Spectra and the Latitude of Surface Westerlies: Interannual Variability and Global Warming Trend, J. Clim., 21, 5942–5959, doi:10.1175/2008JCLI2306.1, 2008.

Ciasto, L. M., Li, C., Wettstein, J. J., and Kvamstø, N. G.: North Atlantic Storm-Track Sensitivity to Projected Sea Surface Temperature: Local versus Remote Influences, J. Clim., 29, 6973–6991, doi:10.1175/JCLI-D-15-0860.1, 2016.

Collins, M., Knutti, R., Arblaster, J., Dufresne, J.-L., Fichefet, T., Friedlingstein, P., Gao, X., Gutowski, W., Johns, T., Krinner, G., Shongwe, M., Tebaldi, C., Weaver, A., and Wehner, M.: Chapter 12 - Long-term climate change: Projections, commitments and irreversibility, in: Climate Change 2013: The Physical Science Basis. IPCC Working Group I Contribution to AR5, edited by IPCC, Cambridge University Press, Cambridge, http://pure.iiasa.ac.at/10551/, 2013.

Dee, D. P., Uppala, S. M., Simmons, A. J., Berrisford, P., Poli, P., Kobayashi, S., Andrae, U., Balmaseda, M. A., Balsamo, G., Bauer, P., Bechtold, P., Beljaars, A. C. M., van de Berg, L., Bidlot, J., Bormann, N., Delsol, C., Dragani, R., Fuentes, M., Geer, A. J., Haimberger, L., Healy, S. B., Hersbach, H., Hólm, E. V., Isaksen, L., Kållberg, P., Köhler, M., Matricardi, M., McNally, A. P., Monge-Sanz, B. M., Morcrette, J.-J., Park, B.-K., Peubey, C., de Rosnay, P., Tavolato, C., Thépaut, J.-N., and Vitart, F.: The ERA-Interim reanalysis: configuration and performance of the data assimilation system, Quarterly Journal of the Royal Meteorological Society, 137, 553–597, doi:10.1002/qj.828, http://dx.doi.org/10.1002/qj.828, 2011.

Delcambre, S. C., Lorenz, D. J., Vimont, D. J., and Martin, J. E.: Diagnosing Northern Hemisphere Jet Portrayal in 17 CMIP3 Global Climate Models: Twenty-First-Century Projections, J. Clim., 26, 4930–4946, doi:10.1175/JCLI-D-12-00359.1, 2013.

Deser, C., Phillips, A., Bourdette, V., and Teng, H.: Uncertainty in climate change projections: the role of internal variability, Clim. Dyn., 38, 527–546, 2012.

Eichler, T. P., Gaggini, N., and Pan, Z.: Impacts of global warming on Northern Hemisphere winter storm tracks in the CMIP5 model suite, Journal of Geophysical Research: Atmospheres, 118, 3919–3932, doi:10.1002/jgrd.50286, http://dx.doi.org/10.1002/jgrd.50286, 2013.

Folland, C., Stone, D., Frederiksen, C., Karoly, D., and Kinter, J.: The international CLIVAR Climate of the 20th Century Plus (C20C+) Project: Report of the sixth workshop, CLIVAR Exchange, 19, 57–59, 2014.

Gerber, E. P. and Son, S.-W.: Quantifying the Summertime Response of the Austral Jet Stream and Hadley Cell to Stratospheric Ozone and Greenhouse Gases, J. Clim., 27, 5538–5559, doi:10.1175/JCLI-D-13-00539.1, 2014.

Graff, L. S. and LaCasce, J. H.: Changes in the Extratropical Storm Tracks in Response to Changes in SST in an AGCM, J. Clim., 25, 1854–1870, doi:10.1175/JCLI-D-11-00174.1, 2012.

Haarsma, R. J. and Selten, F.: Anthropogenic changes in the Walker circulation and their impact on the extratropical planetary wave structure in the Northern Hemisphere, Clim. Dyn., 39, 1781–1799, 2012.

Harvey, B. J., Shaffrey, L. C., Woollings, T. J., Zappa, G., and Hodges, K. I.: How large are projected 21st century storm track changes?, Geophysical Research Letters, 39, n/a–n/a, doi:10.1029/2012GL052873, http://dx.doi.org/10.1029/2012GL052873, l18707, 2012.

Harvey, B. J., Shaffrey, L. C., and Woollings, T. J.: Equator-to-pole temperature differences and the extra-tropical storm track responses of the CMIP5 climate models, Climate Dynamics, 43, 1171–1182, doi:10.1007/s00382-013-1883-9, https://doi.org/10.1007/s00382-013-1883-9, 2014.

Harvey, B. J., Shaffrey, L. C., and Woollings, T. J.: Deconstructing the climate change response of the Northern Hemisphere wintertime storm tracks, Clim. Dyn., 45, 2847–2860, 2015.

Held, I. M. and Soden, B. J.: Robust Responses of the Hydrological Cycle to Global Warming, J. Clim., 19, 5686–5699, doi:10.1175/JCLI3990.1, 2006.

Iversen, T., Bentsen, M., Bethke, I., Debernard, J. B., Kirkevåg, A., Seland, Ø., Drange, H., Kristjansson, J. E., Medhaug, I., Sand, M., and Seierstad, I. A.: The Norwegian Earth System Model, NorESM1-M Part 2: Climate response and scenario projections, Geoscientific Model Development, 6, 389–415, doi:10.5194/gmd-6-389-2013, https://www.geosci-model-dev.net/6/389/2013/, 2013.

Iversen, T., Bethke, I., Debernard, J. B., Graff, L. S., Øyvind Seland, Bentsen, M., Kirkevåg, A., Li, C., and Olivié, D. J. L.: The "NorESM1-Happi" used for evaluating differences between a global warming of 1.5°C and 2°C, and the role of Arctic Amplification, Earth Syst. Dynam., submitted 2017.

Jacob, D., Kotova, L., Teichmann, C., Sobolowski, S., Robert Vautard3, C. D., Koutroulis, A. G., Grillakis, M. G., Tsanis, I. K., Andrea Damm6, A. S., and van Vliet, M. T.: Climate impacts in Europe under +1.5°C global warming, Earth's Future, submitted 2017.

Kidston, J., Vallis, G. K., Dean, S. M., and Renwick, J. A.: Can the Increase in the Eddy Length Scale under Global Warming Cause the Poleward Shift of the Jet Streams?, J. Clim., 24, 3764–3780, doi:10.1175/2010JCLI3738.1, 2011.

Kirkevåg, A., Iversen, T., Seland, Ø., Hoose, C., Kristjánsson, J. E., Struthers, H., Ekman, A. M. L., Ghan, S., Griesfeller, J., Nilsson, E. D., and Schulz, M.: Aerosol-climate interactions in the Norwegian Earth System Model - NorESM1-M, 6, 207–244, doi:10.5194/gmd-6-207-2013, https://www.geosci-model-dev.net/6/207/2013/, 2013.

Kottek, M., Grieser, J., Beck, C., Rudolf, B., and Rubel, F.: World Map of the Köppen-Geiger climate classification updated, Meteorol. Z., 15, 259–263, doi:10.1127/0941-2948/2006/0130, 2006.

Lierhammer, L., Mauritsen, T., Legutke, S., Esch, M., Wieners, K.-H., and Saeed, F.: Simulations of HAPPI (Half a degree Additional warming, Prognosis and Projected Impacts) Tier-1 experiments based on the ECHAM6.3 atmospheric model of the Max Planck Institute for Meteorology (MPI-M), http://cera-www.dkrz.de/WDCC/ui/Compact.jsp?acronym=HAPPI-MIP-global-ECHAM6.3, 2017.

Lorenz, D. J. and DeWeaver, E. T.: Tropopause height and zonal wind response to global warming in the IPCC scenario integrations, J. Geophys. Res., 112, n/a–n/a, doi:10.1029/2006JD008087, http://dx.doi.org/10.1029/2006JD008087, d10119, 2007.

Lu, J., Vecchi, G., and Reichler, T.: Expansion of the Hadley cell under global warming, Geophys. Res. Lett., 34, L06 805, 2007.

Lu, J., Chen, G., and Frierson, D. M. W.: The Position of the Midlatitude Storm Track and Eddy-Driven Westerlies in Aquaplanet AGCMs, J. Atmos. Sci., 67, 3984–4000, doi:10.1175/2010JAS3477.1, 2010.

Michel, C. and Rivière, G.: Sensitivity of the Position and Variability of the Eddy-Driven Jet to Different SST Profiles in an Aquaplanet General Circulation Model, J. Atmos. Sci., 71, 349–371, doi:10.1175/JAS-D-13-074.1, 2014.

Mitchell, D.: Extreme heat-related mortality under targeted Paris Agreement scenarios, Nature Clim. Change, in review 2017.

Mitchell, D., AchutaRao, K., Allen, M., Bethke, I., Beyerle, U., Ciavarella, A., Forster, P. M., Fuglestvedt, J., Gillett, N., Haustein, K., Ingram, W., Iversen, T., Kharin, V., Klingaman, N., Massey, N., Fischer, E., Schleussner, C.-F., Scinocca, J., Seland, Ø., Shiogama, H., Shuckburgh, E., Sparrow, S., Stone, D., Uhe, P., Wallom, D., Wehner, M., and Zaaboul, R.: Half a degree additional warming, prognosis and projected impacts (HAPPI): background and experimental design, Geoscientific Model Development, 10, 571–583, doi:10.5194/gmd-10-571-2017, https://www.geosci-model-dev.net/10/571/2017/, 2017.

Neale, R. B., Richter, J., Park, S., Lauritzen, P. H., Vavrus, S. J., Rasch, P. J., and Zhang, M.: The Mean Climate of the Community Atmosphere Model (CAM4) in Forced SST and Fully Coupled Experiments, J. Clim., 26, 5150–5168, doi:10.1175/JCLI-D-12-00236.1, 2013.

Sanderson, B. M., Xu, Y., Tebaldi, C., Wehner, M., O'Neill, B., Jahn, A., Pendergrass, A. G., Lehner, F., Strand, W. G., Lin, L., Knutti, R., and Lamarque, J. F.: Community climate simulations to assess avoided impacts in 1.5 and 2 °C futures, Earth Syst. Dynam., 8, 827–847, doi:10.5194/esd-8-827-2017, https://www.earth-syst-dynam.net/8/827/2017/, 2017.

Sansom, P. G., Stephenson, D. B., Ferro, C. A. T., Zappa, G., and Shaffrey, L.: Simple Uncertainty Frameworks for Selecting Weighting Schemes and Interpreting Multimodel Ensemble Climate Change Experiments, J. Clim., 26, 4017–4037, doi:10.1175/JCLI-D-12-00462.1, 2013.

Seager, R., Neelin, D., Simpson, I., Liu, H., Henderson, N., Shaw, T., Kushnir, Y., Ting, M., and Cook, B.: Dynamical and Thermodynamical Causes of Large-Scale Changes in the Hydrological Cycle over North America in Response to Global Warming, J. Clim., 27, 7921–7948, doi:10.1175/JCLI-D-14-00153.1, 2014.

Selten, F. M., Branstator, G. W., Dijkstra, H. A., and Kliphuis, M.: Tropical origins for recent and future Northern Hemisphere climate change, Geophys. Res. Lett., 31, n/a–n/a, doi:10.1029/2004GL020739, http://dx.doi.org/10.1029/2004GL020739, l21205, 2004.

Shaw, T. A., Baldwin, M., Barnes, E. A., Caballero, R., Garfinkel, C. I., Hwang, Y.-T., Li, C., O'Gorman, P. A., Rivière, G., Simpson, I. R., and Voigt, A.: Storm track processes and the opposing influences of climate change, Nature Geosci., 9, 656–664, doi:doi:10.1038/ngeo2783, 2016.

Shepherd, T. G.: Atmospheric circulation as a source of uncertainty in climate change projections, Nature Geosci., 7, 703–708, doi:10.1038/NGEO2253, 2014.

Shiogama, H.: 1.5°C goal of Paris agreement will reduce inequities in extreme climate hazards, Nature Clim. Change, submitted 2017.

Shiogama, H., Watanabe, M., Imada, Y., Mori, M., Ishii, M., and Kimoto, M.: An event attribution of the 2010 drought in the South Amazon region using the MIROC5 model, Atmospheric Science Letters, 14, 170–175, doi:10.1002/asl2.435, http://dx.doi.org/10.1002/asl2.435, 2013.

Simpson, I. R., Shaw, T. A., and Seager, R.: A Diagnosis of the Seasonally and Longitudinally Varying Midlatitude Circulation Response to Global Warming, J. Atmos. Sci., 71, 2489–2515, doi:10.1175/JAS-D-13-0325.1, 2014.

Simpson, I. R., Seager, R., Ting, M., and Shaw, T. A.: Causes of change in Northern Hemisphere winter meridional winds and regional hydroclimate, Nature Clim. Change, 6, 65–70, doi:doi:10.1038/nclimate2783, 2016.

Stone, D., Christidis, N., Folland, C., Perkins-Kirkpatrick, S., Perlwitz, J., Shiogama, H., Wehner, M. F., Wolski, P., Cholia, S., Krishnan, H., Murray, D., Angélil, O., Beyerle, U., Ciavarella, A., Dittus, A., Quan, X.-W., and Tadross, M.: Experiment design of the International CLIVAR C20C+ Detection and Attribution Project, in prep 2017.

Trenberth, K. E. and Stepaniak, D. P.: Covariability of components of poleward atmospheric energy transports on seasonal and interannual timescales, J. Clim., 16, 3691–3705, 2003.

Ulbrich, U., Pinto, J., Kupfer, H., Leckebusch, G., Spangehl, T., and Reyers, M.: Changing Northern Hemisphere Storm Tracks in an Ensemble of IPCC Climate Change Simulations, J. Clim., 21, 1669–1679, doi:10.1175/2007JCLI1992.1, 2008.

von Salzen, K., Scinocca, J. F., McFarlane, N. A., Li, J., Cole, J. N. S., Plummer, D., Verseghy, D., Reader, M. C., Ma, X., Lazare, M., and Solheim, L.: The Canadian Fourth Generation Atmospheric Global Climate Model (CanAM4). Part I: Representation of Physical Processes, Atmosphere-Ocean, 51, 104–125, doi:10.1080/07055900.2012.755610, 2013.

Wehner, M., Stone, D., Mitchell, D., Shiogama, H., Fischer, E., Graff, L., Kharin, V., Lierhammer, L., Sanderson, B., and Krishnan, H.: Changes in extremely hot days under stabilized 1.5°C and 2.0°C global warming scenarios as simulated by the HAPPI multi-model ensemble, Earth Syst. Dynam. Discuss., doi:10.5194/esd-2017-89, in review 2017.

Woollings, T. and Blackburn, M.: The North Atlantic Jet Stream under Climate Change and Its Relation to the NAO and EA Patterns, J. Clim., 25, 886–902, doi:10.1175/JCLI-D-11-00087.1, 2012.

Woollings, T., Hannachi, A., and Hoskins, B.: Variability of the North Atlantic eddy-driven jet stream, Q. J. R. Meteorol. Soc., 136, 856–868, doi:10.1002/qj.625, http://dx.doi.org/10.1002/qj.625, 2010.

Woollings, T., Gregory, J., Pinto, J., Reyers, M., and Brayshaw, D.: Response of the North Atlantic storm track to climate change shaped by ocean-atmosphere coupling, Nature Geosci., 5, 313–317, doi:doi:10.1038/ngeo1438, 2012.

Yin, J. H.: A consistent poleward shift of the storm tracks in simulations of 21st century climate, Geophys. Res. Lett., 32, n/a–n/a, doi:10.1029/2005GL023684, http://dx.doi.org/10.1029/2005GL023684, l18701, 2005.

Zappa, G., Shaffrey, L. C., Hodges, K. I., Sansom, P. G., and Stephenson, D. B.: A Multimodel Assessment of Future Projections of North Atlantic and European Extratropical Cyclones in the CMIP5 Climate Models, J. Clim., 26, 5846–5862, doi:10.1175/JCLI-D-12-00573.1, 2013.

Zappa, G., Hawcroft, M., Shaffrey, L., Black, E., and Brayshaw, D.: Extratropical cyclones and the projected decline of winter mediterranean precipitation in the CMIP5 models, Clim. Dyn., 45, 1727–38, 2015a.

Zappa, G., Hoskins, B. J., and Shepherd, T. G.: The dependence of wintertime Mediterranean precipitation on the atmospheric circulation response to climate change, Environ. Res. Lett., 10, 104 012, doi:10.1088/1748-9326/10/10/104012, 2015b.